DENSITY DISTRIBUTIONS OF ^{8}Li ON PROTON TARGET

G.W. Fan, Shuai Cao

School of Chemical Engineering
Anhui University of Science and Technology
Huainan, 232001, China

Received 30 January 2024, accepted 7 March 2024, published online 14 March 2024

We have measured reaction cross sections of neutron-rich ^{8}Li nucleus on proton target at intermediate energies from 40.9 to 105.4 MeV/nucleon using the transmission method. Density distributions of ^{8}Li are deduced by the use of the Glauber model to fit the experimental data. The matter and neutron radii converted from densities are consistent with other previous measurements. This work suggests that the measurement of the reaction cross section on the proton target can be a method to extract the neutron density distribution or neutron radius.

DOI:10.5506/APhysPolB.55.3-A1

1. Introduction

The nucleus is a complex system governed by the laws of quantum mechanics, and until now, is full of mysteries due to difficulties in solving many-body problems exactly. Nuclear physicists in reality select a different approach rather than build an exact replica of the complex system. They describe the properties of the nucleus using several approximate methods, such as the relativistic mean field theory [1] and cluster theory [2]. A relatively small number of measurable properties are chosen to compare with the experimental results, and then as bridges in the theory to reveal the overall characteristics of the entire nucleus. The root-mean-square radius is such a basic property.

The root-mean-square radius of the neutron (r_n) is essential when a neutron-rich nucleus is discussed. The neutron skin thickness, defined as $\Delta r_{np} = r_n - r_p$, where r_p is the root-mean-square radius of the proton, helps to determine the equation of state at low temperatures [3–6] and even to explore the neutron stars and stellar explosions [7]. Besides, the r_p measurement of the neutron-rich nuclei has further confirmed some hidden information in the neutron-halo nucleus, the valence neutron(s) changes the charge

distributions of the core nucleus as compared to the corresponding nucleus without the valence neutron(s), and the difference reflects the information on the interactions between different subsystems of the strongly clustered nucleus, which might originate from the motion of the core relative to the center of mass and the core polarization [8–18]. Systematic measurement of radii of the neutron-rich nuclei will be of great help to uncover the hidden information. Therefore, many experiments have been performed to develop a consistent picture of the neutron-rich nuclei [19–21].

The neutron-rich ^{8}Li nucleus with a small separation energy $S_n = 2.0$ MeV for p-state valence neutron has been studied many times. Its surface neutron density is important to the $^{7}\mathrm{Li}(n,\gamma)^{8}\mathrm{Li}$ reaction, which is considered to be a key reaction in jumping the $A = 8$ gap in the nucleosynthesis [22]. Several theories have been employed to investigate the reaction or the ^{8}Li structure, such as the cluster model [23], the shell model [24], the relativistic mean field [25], and the Hartree–Fock method [26]. However, there is an obvious difference in the calculation results. Thus, it is necessary to extract the neutron distribution or r_n directly from the experiment.

The birth of the Radioactive Ion-Beams (RIBs) technique extremely promotes the development of nuclear structure physics, in particular the unstable nuclei. One of the methods with RIBs is the measurement of the reaction cross section (σ_{R}) and then fitting the experimental data with the Glauber model. The Glauber model connects the σ_{R} to the nuclear density distributions. In order to extract radii of ^{8}Li, we measured the σ_{R} on a proton target at intermediate energies from 40.9 to 105.4 MeV/nucleon using the transmission method. In the following section, we will briefly explain the experiment. A framework of the Glauber model and density distributions of ^{8}Li extracted will be shown in Section 3, which is followed by a summary in Section 4.

2. Experiment

The experiment was carried out using the Heavy Ion Medical Accelerator in Chiba (HIMAC) synchrotron and the fragment-separator facility at the National Institute of Radiological Sciences (NIRS), Japan. Four kinds of reaction targets, ^{12}C, ^{9}Be, ^{27}Al, and CH_2, were used at the same time, a part of the results was already published in [27]. In this paper, we mainly analyzed the measurements with ^{12}C and CH_2, which were combined to get a proton target through the equation of σ_{R} on proton = (σ_{R} on $CH_2 - \sigma_{\mathrm{R}}$ on ^{12}C)/2. Figure 1 (a) shows the schematic drawing of the experimental setup. A ^{13}C primary beam with 130 MeV/nucleon and a ^{9}Be production target were used to produce the secondary beam of ^{8}Li through the projectile-fragmentation reaction. Secondary beams with energies from 40.9 to 105.4 MeV/nucleon

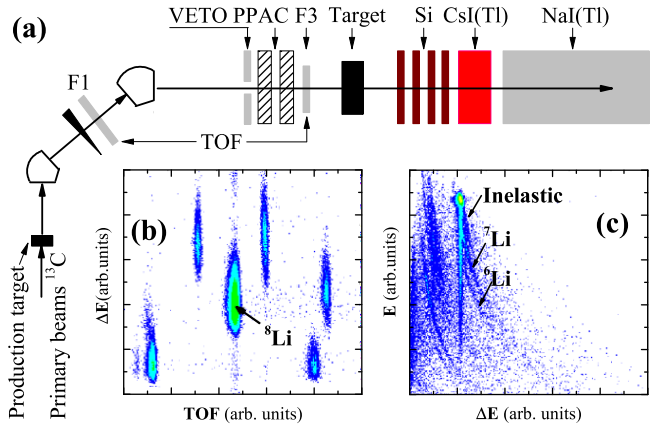

Fig. 1. (a) Schematic drawing of the experimental setup. (b) and (c) Typical particle identification spectra.

were obtained by tuning the thickness of the production target and parameters of the accelerator NIRS. Particles before the reaction target were identified with the ΔE–TOF, the ΔE was recorded by ab F3 plastic detector ($20.0 \times 20.0 \times 0.4$ mm^3). The F1 plastic detector ($40.0 \times 40.0 \times 0.4$ mm^3) and the F3 provided the TOF. A VETO plastic scintillator ($100 \times 100 \times 1$ mm^3) with a $\oslash$19-mm hole was placed in the center on the beam-line axis to avoid pileup events. The events occurring within a 10 μs time gate between the F3 and VETO were looked at as pileup events and would be rejected in the offline analysis. Two position-sensitive gas counters, parallel plate avalanche counters (PPAC), were used to record the position of the beams. The effect working area of the PPAC is 100×100 mm^2. Figure 1 (b) shows a typical result of the particle identification before the reaction target. Particles after the reaction target were identified with the $\Delta E - E$. The energy-deposition ΔE was recorded by four Si detectors ($50.0 \times 50.0 \times 0.5$ mm^3) combined with a CsI(Tl) detector ($50.0 \times 50.0 \times 3$ mm^3). A NaI(Tl) scintillation counter ($\oslash 76.2 \times 60.0$ mm^2) recorded the remaining energy E of outgoing particles after the CsI(Tl) detector. Besides, we also performed a target-out measurement to correct the reactions outside the target and mainly the reactions in the Si, CsI(Tl), and NaI(Tl) detectors. Figure 1 (c) shows particle identifications after the reaction target.

The σ_{R} was obtained with an equation of $\sigma_{\mathrm{R}} = -1/t \times \ln(R_{\mathrm{in}}/R_{\mathrm{out}})$, where t denotes the thickness of the reaction target, R_{in} denotes the ratio of the outgoing ^{8}Li events to that of incident events for the target-in measurement, and R_{out} is the same ratio for the target-out measurement.

3. Glauber model and calculations

The Glauber model is a semi-classical scattering theory based on the eikonal approximation [28]. The main equations for nucleon–nucleus scattering are described as follows:

$$\sigma_{\mathrm{R}} = 2\pi \int b\,\mathrm{d}\,b \left[1 - \mathrm{e}^{-2Im\chi(b)}\right] C(E)\,, \tag{1}$$

where $C(E)$ denotes the influence of the Coulomb force [29] and b is an impact parameter. $\chi(b)$ is expressed as

$$\chi(b) = i \int \mathrm{d}s \Gamma_{NN}(b-s)\rho(s)\,, \tag{2}$$

where Γ is the profile function, ρ is the z-integrated density of the projectile, and s is the nucleon perpendicular to the beam axis. In fact, ρ is divided into proton density distribution ρ_p and neutron density distribution ρ_n. Therefore, Eq. (2) can also be written as

$$\chi(b) = i \left(\int \mathrm{d}s \Gamma_{pp}(b-s)\rho_p(s) + \int \mathrm{d}s \Gamma_{np}(b-s)\rho_n(s) \right). \tag{3}$$

Γ is parametrized as

$$\Gamma_{NN}(b) = \tfrac{1-i\alpha}{4\pi\beta}\sigma_{NN}(E) \exp\left(-\tfrac{b^2}{2\beta}\right), \tag{4}$$

where $\sigma_{NN}(E)$ is the nucleon–nucleon total cross section at kinetic energy E [29], β is the finite-range parameter, and α is the ratio of the real and imaginary parts of the NN-scattering amplitude. In this work, we set $\alpha = 0$, and $\beta = \sigma_{NN}/16\pi (E < 300$ MeV/nucleon) and 0.14 fm^2 ($E \geq 300$ MeV/nucleon) [30]. In fact, if ρ_p or charge radius is settled, ρ_n can be extracted.

In the scattering theory, it is very difficult to accurately solve the Schrödinger equation, hence it is assumed that the incident particle has high energy, the wave function will oscillate rapidly, and its deviation from a plane wave can be expected to be small. Thus, the Glauber model has been proved successful in high-energy scattering. As the energy of the incident

particle decreases, the oscillation of the wave function slows down, the influence of the Fermi motion of nucleons becomes more and more significant, therefore, it is necessary to add the Fermi motion to this calculation [30]. In the modification, the σ_{NN} is corrected as

$$\sigma_{NN}^{\text{eff}} = \int \mathrm{d}\, p_{\text{rel}} \sigma_{NN} D(p_{\text{rel}})\,, \tag{5}$$

$$D(p_{\text{rel}}) = \frac{1}{\sqrt{2\pi\left(p_p^2\right)}} \exp\left[-\frac{(p_{\text{rel}}-p_{\text{proj}})^2}{2\pi\left(p_p^2\right)}\right], \tag{6}$$

where p_{proj} denotes the momentum of a nucleon with the same velocity as the projectile, p_p^2 is a mean square momentum of a nucleon in the projectile, for ^{8}Li, we used the value of 90 and 38.7 MeV/c like that of ^{8}B [30, 31].

The shape of the density distribution is always restricted by the functional shape chosen. Thus, it is necessary to assume ^{8}Li density shapes with several free parameters. We chose a harmonic oscillator (HO) shape for the stable part and a Yukawa function for the valence part. The shapes are expressed as follows:

The HO-type function.

$$\rho_c^i(r) = \rho_0 \left[1 + \tfrac{c-2}{3}\left(\tfrac{r}{b}\right)^2\right] \exp\left[-\left(\tfrac{r}{b}\right)^2\right], \tag{7}$$

where I denotes the proton or neutron, 'c' is the number of protons or neutrons in the core, b describes the width, and ρ_0 is the normalization factor. In the analysis, we set $b = 1.59 \pm 0.02$ fm to reproduce the charge radius of ^{8}Li [9].

The Yukawa function.

$$\rho(r) = \begin{cases} X\rho_c(r)\,, & r \le r_c\,, \\ Y\frac{\exp(-\lambda r)}{r^2}\,, & r > r_c\,, \end{cases} \tag{8}$$

where r_{c} is the intersection point of the core and the tail part, X and Y are the normalization factors, and λ is the tail slope.

Figures 2 and 3 show best-fit σ_{R} and density distributions. In the calculation, three protons and four neutrons in the core were taken as a stable part which is described with the HO shape, the valence neutron is described with the Yukawa function. The reduced χ^2 is 0.22. The best-fit parameters are $\lambda = 0.86 \pm 0.04$ fm^{-1} and $Y/X = 8.14 \pm 0.06$. The matter radius is 2.43 ± 0.06 fm, which is consistent with the previous results on stable nucleus targets ($r_m = 2.39 \pm 0.05$ fm [27] and 2.51 ± 0.03 fm [32]). In order to further test the reliability, we also do the calculation only with the HO function ($b = 1.59 \pm 0.02$ fm). As shown in Fig. 2, the calculation obviously

underestimates the σ_{R}. It also suggests the necessity of the valence tail part like in previous results, see Fig. 3. Therefore, the calculations indicate that this method to get a proton target (σ_{R} on proton = (σ_{R} on $CH_2 - \sigma_{\mathrm{R}}$ on ^{12}C)/2) and to extract the density distribution is reasonable.

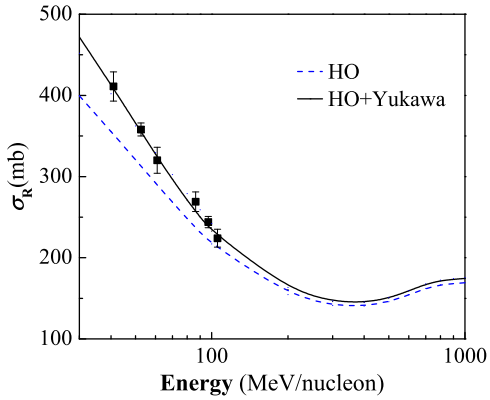

Fig. 2. The experimental and best-fit σ_{R} of ^{8}Li on proton target.

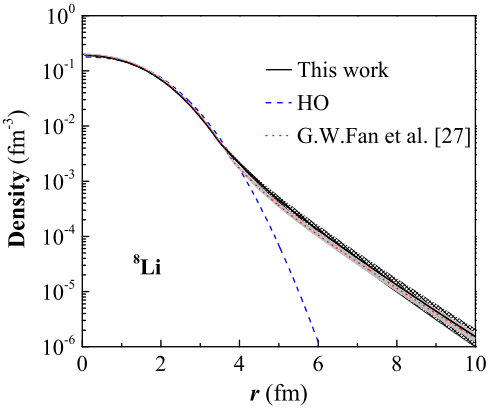

Fig. 3. Matter density distributions of ^{8}Li, the solid curve with the square pattern is for this work.

The r_n and neutron density distribution are also extracted in this work, and the results are shown in Figs. 4 and 5. We can see that the $r_n (= 2.60 \pm 0.06$ fm) of this work is consistent with the measurement on ^{12}C target [32]. It indicates that this work is reasonable and feasible. The neutron density distribution clearly shows a tail structure in ^{8}Li. However, the area of the tail from the connection point is only 1.25% of the total. It means a small tail. In general, it is difficult to extract the neutron density distribution

through the σ_{R} due to the limitation of the Glauber theory. Thanks to the development of new technologies, such as high-precision laser spectroscopy and the measurement of the charge-changing cross section, allowing to get the r_p, extracting of the neutron density distribution can be achieved.

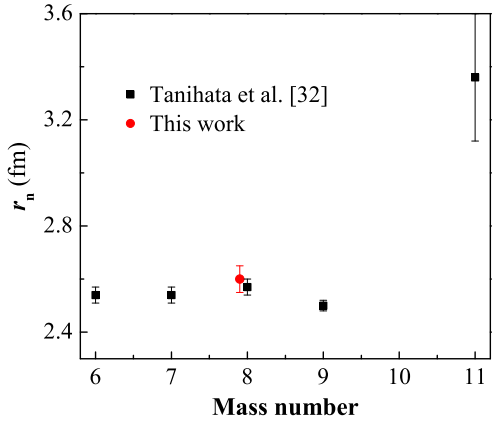

Fig. 4. Radii of ^{8}Li, the solid circle is for this work.

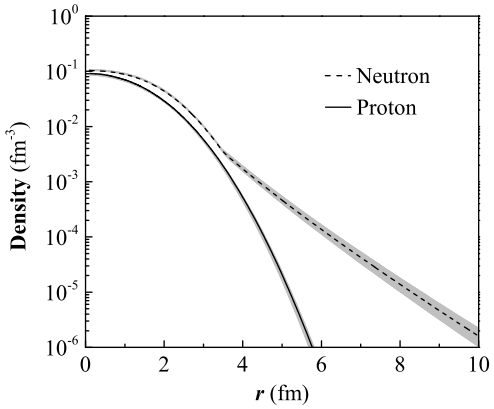

Fig. 5. Density distributions of ^{8}Li. The dashed curve is for neutrons.

4. Conclusion

The σ_{R} of ^{8}Li on proton has been measured at energies from 40.9 to 105.4 MeV/nucleon with the method of σ_{R} on proton = (σ_{R} on $CH_2 - \sigma_{\mathrm{R}}$ on ^{12}C)/2. Based on the Glauber-type analysis, we have deduced density distributions, especially neutron density distribution of ^{8}Li. The present study may open up an approach to get a proton target in this field.

The authors thank the AEC staff for their technical support and excellent accelerator operations, the M. Fukuda's group of the Osaka University, the T. Yamaguchi's group of the Saitama University, and the S. Suzuki's group of the Niigata University for their help in this experiment. This work was supported by the following foundations: the Anhui Provincial Natural Science Foundation (2008085MA17) and the Foundation of Anhui University of Science and Technology grant No. 11130.

REFERENCES

[1] P.G. Reinhard, «The relativistic mean-field description of nuclei and nuclear dynamics», *Rep. Prog. Phys.* **52**, 439 (1989).

[2] K. Varga, Y. Suzuki, I. Tanihata, «Microscopic four-cluster description of the mirror nuclei ^{9}Li and ^{9}C», *Phys. Rev. C* **52**, 3013 (1995).

[3] L.W. Chen, C.M. Ko, B.A. Lietal., «Density slope of the nuclear symmetry energy from the neutron skin thickness of heavy nuclei», *Phys. Rev. C* **82**, 024321 (2010).

[4] X. Roca-Maza *et al.*, «Neutron Skin of ^{208}Pb, Nuclear Symmetry Energy, and the Parity Radius Experiment», *Phys. Rev. Lett.* **106**, 252501 (2011).

[5] M. Kortelainen *et al.*, «Neutron-skin uncertainties of Skyrme energy density functionals», *Phys. Rev. C* **88**, 031305(R) (2013).

[6] T. Inakura, T. Nakatsukasa, K. Yabana, «Low-energy *E1* strength in select nuclei: Possible constraints on neutron skin and symmetry energy», *Phys. Rev. C* **88**, 051305(R) (2013).

[7] P.B. Demorest *et al.*, «A two-solar-mass neutron star measured using Shapiro delay», *Nature* **467**, 1081 (2010).

[8] L.-B. Wang *et al.*, «Laser Spectroscopic Determination of the ^{6}He Nuclear Charge Radius», *Phys. Rev. Lett.* **93**, 142501 (2004).

[9] R. Sánchez, W. Nörtershäuser, G. Ewaldetal, «Nuclear Charge Radii of ^{9,11}Li: The Influence of Halo Neutrons», *Phys. Rev. Lett.* **96**, 033002 (2006).

[10] P. Mueller *et al.*, «Nuclear Charge Radius of ^{8}He», *Phys. Rev. Lett.* **99**, 252501 (2007).

[11] A. Krieger *et al.*, «Nuclear Charge Radius of ^{12}Be», *Phys. Rev. Lett.* **108**, 142501 (2012).

[12] W. Nörtershäuser *et al.*, «Nuclear Charge Radii ^{7,9,10}Be of and the One-Neutron Halo Nucleus ^{11}Be», *Phys. Rev. Lett.* **102**, 062503 (2009).

[13] L.V. Chulkov *et al.*, «Total charge-changing cross sections for neutron-rich light nuclei», *Nucl. Phys. A* **674**, 330 (2000).

[14] T. Yamaguchi *et al.*, «Energy-dependent charge-changing cross sections and proton distribution of ^{28}Si», *Phys. Rev. C* **82**, 014609 (2010).

[15] T. Yamaguchi *et al.*, «Scaling of Charge-Changing Interaction Cross Sections and Point-Proton Radii of Neutron-Rich Carbon Isotopes», *Phys. Rev. Lett.* **107**, 032502 (2011).

[16] A. Estradé *et al.*, «Proton Radii of $^{12-17}$B Define a Thick Neutron Surface in ^{17}B», *Phys. Rev. Lett.* **113**, 132501 (2014).

[17] S. Terashima *et al.*, «Proton radius of ^{14}Be from measurement of charge-changing cross sections», *Prog. Theor. Exp. Phys.* **2014**, 101D02 (2014).

[18] R. Kanungo *et al.*, «Proton Distribution Radii of $^{12-19}$C Illuminate Features of Neutron Halos», *Phys. Rev. Lett.* **117**, 102501 (2016).

[19] T. Moriguchi *et al.*, «Density distributions of ^{11}Li deduced from reaction cross-section measurements», *Phys. Rev. C* **88**, 024610 (2013).

[20] T. Moriguchi *et al.*, «Density distribution of ^{14}Be from reaction cross-section measurements», *Nucl. Phys. A* **929**, 83 (2014).

[21] M. Tanaka *et al.*, *JPS Conf. Proc.* **6**, 020026 (2015).

[22] J.E. Lynn, E.T. Jurney, S. Raman, «Direct and valence neutron capture by ^{7}Li», *Phys. Rev. C* **44**, 764 (1991).

[23] K. Varga, Y. Suzuki, I. Tanihata, «Microscopic four-cluster description of the mirror nuclei ^{9}Li and ^{9}C», *Phys. Rev. C* **52**, 3013 (1995).

[24] H. Kitagawa, H. Sagawa, «Quadrupole-moments in mirror nuclei and proton halo», *Phys. Lett. B* **299**, 1 (1993).

[25] S.K. Patra, C.L. Wu, C.R. Praharaj, «Proton-skin in ^{8}B-Nucleus», *Mod. Phys. Lett. A* **13**, 2743 (1998).

[26] Y.S. Shen Z. Ren, «Skyrme–Hartree–Fock calculation on He, Li, and Be isotopes», *Phys. Rev. C* **54**, 1158 (1996).

[27] G.W. Fan *et al.*, «Structure of ^{8}Li from a reaction cross-section measurement», *Phys. Rev. C* **90**, 044321 (2014).

[28] R.J. Glauber, «Lectures on Theoretical Physics», in: W.E. Brittin, L.C. Dunham (Eds.) «Interscience, Vol. 1», New York 1959, p. 315.

[29] B. Abu-Ibrahim, Y. Suzuki, «Scatterings of complex nuclei in the Glauber model», *Phys. Rev. C* **62**, 034608 (2000).

[30] M. Takechi *et al.*, «Reaction cross sections at intermediate energies and Fermi-motion effect», *Phys. Rev. C* **79**, 061601 (2009).

[31] M.H. Smedberg *et al.*, «New results on the halo structure of ^{8}B», *Phys. Lett. B* **452**, 1 (1999).

[32] I. Tanihata *et al.*, «Measurements of Interaction Cross Sections and Nuclear Radii in the Light *p*-Shell Region», *Phys. Rev. Lett.* **55**, 2676 (1985).